JACS
JOURNAL OF THE AMERICAN CHEMICAL SOCIETY
Communication
pubs.acs.org/JACS

Small-Molecule Labeling of Live Cell Surfaces for Three-Dimensional Super-Resolution Microscopy

Marissa K. Lee,[†] Prabin Rai,[‡] Jarrod Williams,[‡] Robert J. Twieg,[‡] and W. E. Moerner*,[†]

[†]Department of Chemistry, Stanford University, Stanford, California 94305, United States
[‡]Department of Chemistry and Biochemistry, Kent State University, Kent, Ohio 44242, United States

Supporting Information

ABSTRACT: Precise imaging of the cell surface of fluorescently labeled bacteria requires super-resolution methods because the size-scale of these cells is on the order of the diffraction limit. In this work, we present a photocontrollable small-molecule rhodamine spirolactam emitter suitable for non-toxic and specific labeling of the outer surface of cells for three-dimensional (3D) super-resolution (SR) imaging. Conventional rhodamine spirolactams photoswitch to the emitting form with UV light; however, these wavelengths can damage cells. We extended photoswitching to visible wavelengths >400 nm by iterative synthesis and spectroscopic characterization to optimize the substitution on the spirolactam. Further, an *N*-hydroxysuccinimide-functionalized derivative enabled covalent labeling of amines on the surface of live *Caulobacter crescentus* cells. Resulting 3D SR reconstructions of the labeled cell surface reveal uniform and specific sampling with thousands of localizations per cell and excellent localization precision in *x*, *y*, and *z*. The distribution of cell stalk lengths (a sub-diffraction-sized cellular structure) was quantified for a mixed population of cells. Pulse-chase experiments identified sites of cell surface growth. Covalent labeling with the optimized rhodamine spirolactam label provides a general strategy to study the surfaces of living cells with high specificity and resolution down to 10−20 nm.

The exterior of a cell is a three-dimensional (3D) biological structure that delineates a barrier for material to enter or exit the cell and defines the overall cell morphology. The growth, shape, and composition of this structure have been studied using fluorescence microscopy of labeled cell surfaces; however, the available resolution is limited by diffraction (~250 nm laterally and ~500 nm axially).[1,2] A class of super-resolution (SR) microscopy methods circumvents the diffraction limit by super-localizing sparse sets of emitting single molecules (SM) separated in time.[3−6] Pooling SM localizations creates a reconstructed image with significantly enhanced resolution on the order of ~10−40 nm.

In order to temporally separate SMs on a densely labeled structure, the fluorescent label must have at least two states with different emissive properties. Transitions between the photophysical states can be driven optically (photoswitching, photoactivation)[7−13] or non-optically (ligand binding, reduction).[6,14−16] Photoswitchable molecules often require the presence of additives like thiols[4,17,18] or redox agents.[19,20]

Photocontrollable fluorescent proteins (FPs)[7,21,22] are frequently used for SR imaging because targeting a specific biological structure is more straightforward than for small organic fluorophores, though new labeling technologies have been developed for the latter.[23] However, the precision of localizing a SM scales as $1/\sqrt{N}$ (where N is the number of photons detected),[24] and organic fluorophores emit on average ~10 times more photons than FPs.[25] An additional advantage of small-molecule fluorophores (~1 kDa) is that they may be less perturbative to the biology than the relatively large FPs (~28 kDa).[26,27]

Rhodamine spirolactams are one class of photocontrollable organic fluorophores. These molecules have two primary isomers: a non-fluorescent, transparent "closed" isomer and a highly fluorescent, colored "open" xanthylium isomer. Absorption of UV light by the closed isomer can break the bond between the lactam nitrogen and the xanthene ring, restoring conjugation in the xanthene ring and generating the fluorescent open isomer (Scheme 1, Figure S1).[28,29] This open isomer emits photons

Scheme 1. Photoswitching of Rhodamine Spirolactam

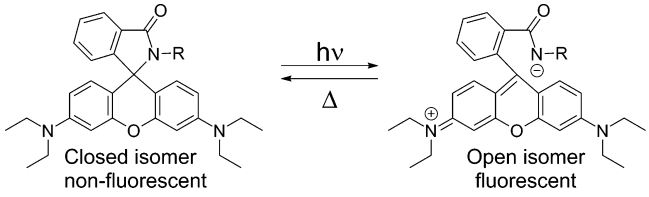

($\lambda_{em}^{max} \approx 580$ nm) until either thermally reverting back to the more stable dark isomer or photobleaching. The time interval before thermal return to the closed isomer depends on the local environment, but it is on the order of milliseconds in polar solvents.[29] The increased stability of the fluorescent form at low pH or in polymers (Figure S2) has been exploited to create chemosensors.[30−32] For cell imaging, UV activation wavelengths have been avoided by using two-photon absorption of IR wavelengths to generate the fluorescent isomer.[8] This imaging strategy not only decreased photodamage but also provided enhanced axial sectioning due to the non-linearity of two-photon absorption.[8]

Received: August 5, 2014
Published: September 15, 2014

   dx.doi.org/10.1021/ja508028h | J. Am. Chem. Soc. 2014, 136, 14003−14006

In this work, we increased the biocompatibility of rhodamine spirolactam derivatives by extending the switching wavelength to the visible region of the spectrum. This allowed the use of a low-intensity, continuous-wave 405 nm laser to photoactivate. Fluorescence was read out using a green (561 nm) laser. An optimized molecule was used to covalently label the surface of live *Caulobacter crescentus* bacterial cells for 3D SR imaging. This straightforward labeling procedure can easily be applied to other cell surfaces.

We hypothesized that varying the chromophore on the lactam nitrogen could lower the energy required to photoactivate without substantially altering the photophysics of the fluorescent isomer. The relative red-shift of each our derivatives (Chart 1)

Chart 1. Rhodamine Spirolactam Derivatives

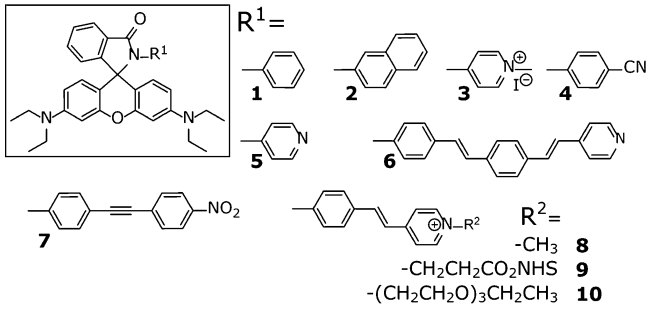

was quantified by integrating the absorbance curve for wavelengths >400 nm (Figure 1). Increased conjugation and

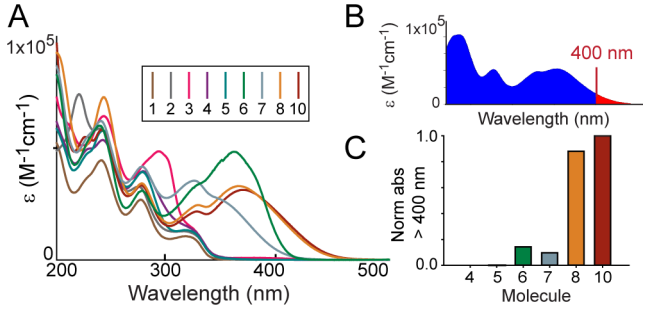

Figure 1. (A) Overlaid absorption spectra of the closed isomer of derivatives **1**–**10** in 1:1 acetonitrile:water. (B) Schematic of absorption integration past 400 nm. Example spectrum is for molecule **8**. (C) Normalized absorption greater than 400 nm for the most red-shifted derivatives.

positive charge on the lactam stilbazolium substituent (**8**–**10**) result in a larger red-shift. Small ring systems (derivatives **1**–**5**) do not absorb appreciably beyond ∼350 nm. Derivatives **6**–**10** are relatively more red-shifted and contain more conjugation. The presence of charge also seems to help stabilize the closed isomer: **8** and **10** are more red-shifted than **6**. Molecules of **8** doped into polymer could be photoactivated using 405 nm light (Figure S2). The photoactivation quantum efficiencies are in the range of 1×10^{-4}–90×10^{-4} (Figure S3, Table S1). As hypothesized, fluorescence emission maxima for all the open derivatives stay fairly constant (∼580 nm), as they all share a common xanthylium ion (Figure S4, Table S1).

Further functionalization of our neutral red-shifted derivatives in combination with a targeting tag could have allowed labeling of internal cellular proteins. Instead, we chose the surface of bacterial cells as our SR target. This demonstration structure avoids issues with dye penetration, specific labeling, and wash-out. Additionally, many SR experiments studying FP-labeled protein super-structures in bacteria would be enhanced with the context of the cell surface.[27] Two-color experiments are possible because rhodamine spirolactams and green or yellow FPs are spectrally separable.

Cell surfaces are inherently 3D, but without additional engineering, SR microscopy only improves the lateral (2D) resolution. One 3D strategy manipulates the point spread function (PSF) of the microscope to encode additional axial (z) information in the shape of the PSF.[33−36] The double-helix (DH)-PSF modulates the emitted light such that the image of a SM now appears as two lobes, with the angle between the lobes encoding axial position.[37−39] Compared to other methods, the DH-PSF is relatively simple to implement, has a large depth of field (∼2 μm), and has a more uniform localization precision in all three dimensions.[40−42]

We labeled the surface amines on the Gram-negative bacterium *C. crescentus* by incubating with nanomolar concentrations of **9** and washing away any unreacted dye. The *N*-hydroxysuccinimide ester on **9** non-specifically labels amines, and the positive charge of **9** also inhibits its entry into the cell. The cells continue to grow normally after labeling. Labeled, live cells are imaged using a low-intensity purple laser (405 nm, 18 W/cm^2 at sample) to activate a low concentration of emitters (Movie S1). Fluorescence is read out using a green laser (561 nm, 1.4 kW/cm^2 at sample). The x, y, and z position of each SM is extracted by fitting (Supporting Information). Thermal drift of the sample over the acquisition time is corrected using a fluorescent bead as a fiduciary marker. Representative raw SM data and the corresponding fits are shown in Figure 2C,D. The 3D SR reconstruction (Figure 2E) of the group of four cells (Figure 2A) contains 4300 ± 500 localizations per cell (∼24 000 frames at 50 ms/frame) with localization precision of ∼14 nm laterally and ∼17 nm axially (Figure S5). The SR data reveal sub-diffraction-sized stalk structures (pink arrows in Figure 2E) not visible with standard microscopy (Figure 2B).

These stalk structures are characteristic of one of the developmental states of *C. crescentus*. This bacterium is a model organism for asymmetric cell division because the two daughter cells differ in their appearance and behavior. Dividing cells are non-motile and contain a stalk at one pole. The nascent daughter cell (termed a swarmer cell) does not divide, is motile, and contains a single flagellum at one pole.[43] The surface of these cells is unusual because besides the usual Gram-negative layers, the exterior of the cell is protected by a surface S-layer composed of a semi-crystalline matrix of a protein called RsaA.[44]

Since this population of cells is in a mixture of developmental states and generations, a variety of stalk lengths can be observed (Figure 3). The average stalk length is 1.3 ± 0.1 μm (measured for 44 cells). Some cells exhibit exceptionally long stalks (see cell 7 in Figure 3A). Prior electron microscopy (EM) measured the thickness of the stalk to be ∼100–200 nm.[45] The mean cross-sectional stalk thickness of our 3D SR reconstructions has a fwhm of ∼104 nm (σ = 44 ± 0.5 nm, 48 stalks) (Figure S6). Assuming only the surface of the stalk is labeled, the underlying structure should be a hollow tube. This is not captured in our data because of the finite localization precision, a fact that has been verified by simulation (Figure S7).

The surface specificity of **9** is more evident in reconstructions of the cell body. The number of localizations found inside the cell volume represents ∼2% of the total number of localizations on the surface. Figure 4A highlights a 75 nm slice of localizations

dx.doi.org/10.1021/ja508028h | J. Am. Chem. Soc. 2014, 136, 14003−14006

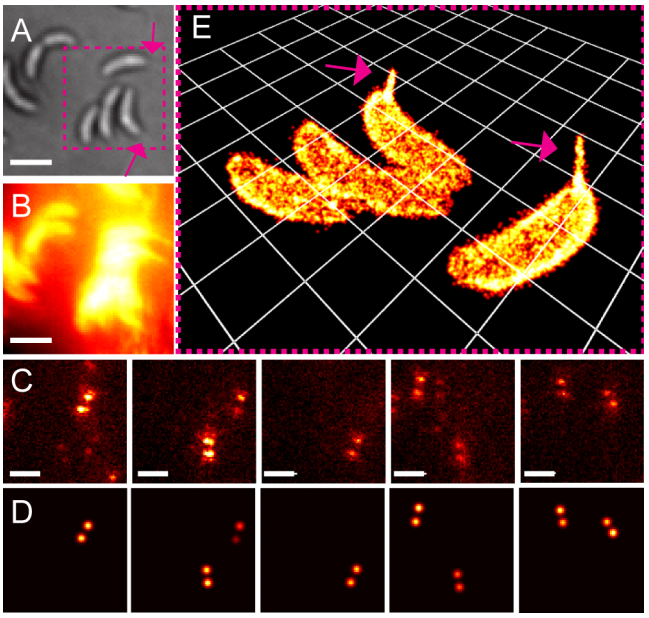

Figure 2. (A) Transmission image of six *C. crescentus* cells from white-light illumination. (B) Diffraction-limited fluorescence image showing average fluorescence over ~20 000 frames (50 ms integration time per frame). (C) Individual frames of raw data showing single molecules (SMs). Since the double-helix phase mask is in place, each SM appears as two spots, with the angle between the spots encoding axial position. (D) Corresponding fitted SMs. (E) Three-dimensional reconstructed image of the four cells in the pink dashed rectangle in panel A. Arrows in panels A and E guide the eye to the cell stalk, a sub-diffraction-sized structure. Localizations were acquired over ~24 000 frames at 50 ms/frame (~20 min total). All scale bars are 1 μm. See Supporting Information for more information about sample preparation, data acquisition, SM fitting, and super-resolution reconstructions.

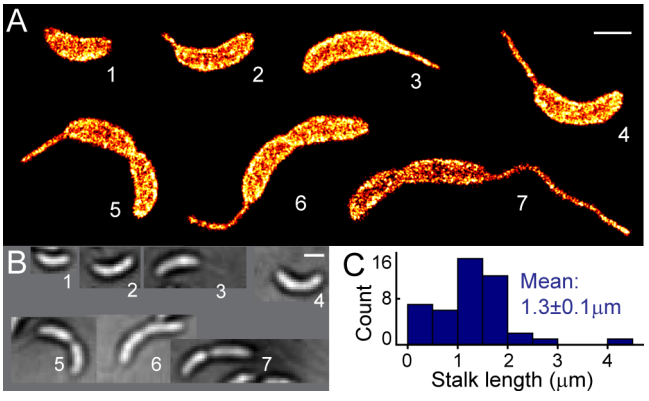

Figure 3. (A) Montage of different stalk lengths in representative cells. Cell 1 does not have a stalk. (B) Corresponding white light image of the cells shown in panel A. (C) Histogram of the measured stalk length.

(yellow) perpendicular to the cell axis. Rotating this slice into the transverse plane shows that the SM positions roughly form a circle of diameter ~300 nm (Figure 4B). The histogram of the radial distance of each localization to the fitted circle center can be fit to a Gaussian with $\sigma = 28$ nm (Figure 4C, Figure S8, Movie S2). The apparent surface thickness is a convolution of the statistical resolution and the true thickness of the underlying structure. The localization precision of the experiment dominates the thickness measurement, suggesting that the underlying sampled structure is much thinner. The thickness of the RsaA layer measured by cryo-EM is ~8 nm.[44] The radial

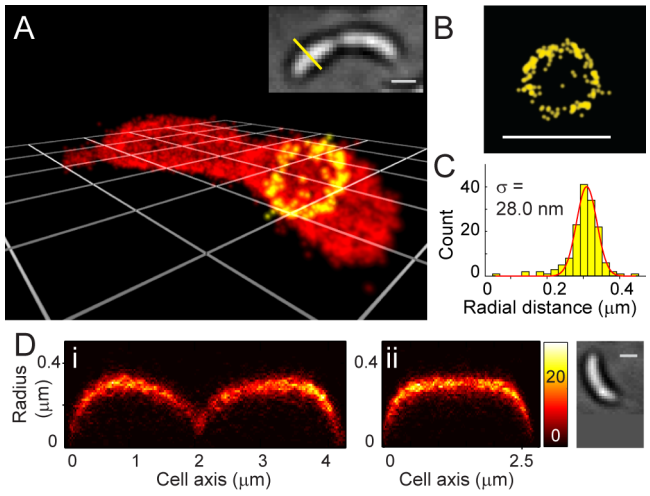

Figure 4. (A) 3D SR reconstruction of surface localizations, with a 75 nm slice highlighted in yellow. Inset: white light image of cell. (B) Yellow section from panel A viewed in the plane of the cell axis. (C) Histogram of the radial distances of each of the localizations (152 localizations total) to the center of the circle fitted to the points in panel B. (D) (i) 2D histogram of radial distances as a function of the long cell axis for the pre-divisional cell shown in panel A. Localizations are binned using a sliding window of 75 nm that slides 25 nm for each data point. (ii) For comparison, histogram of radial distances for a stalked cell (shown in white light image to the far right). Note that this histogram does not have a dip in the center. All scale bars are 1 μm.

distribution of localizations on the cell body varies as a function of the position along the cell axis. For the pre-divisional cell shown in Figure 4D(i), the radii noticeably dip at the interface between the two daughter cells. In comparison, non-dividing cells lack this dip (example in Figure 4D(ii)).

Prior work highlighted the *C. crescentus* surface using the transient binding of a membrane-sensitive dye such as Nile Red in the surrounding solution.[39,42] This method, known as PAINT,[6] can provide ~1000 localizations per cell with precision of ~19 nm (xy) and ~34 nm (z) and a surface thickness of $\sigma \approx 58$ nm. This may be sufficient to provide cellular context, but covalent labeling with **9** provides improved surface labeling. Nile Red is neutral and may have complicated binding kinetics facilitating its interaction with various components of the cell surface, bilayers, and wall. In contrast, **9** is positively charged and therefore excluded from the cell interior. It covalently reacts with and labels surface amines, and unreacted dye can be washed away before imaging. One of the striking differences between the two strategies is the greater sampling uniformity of **9** with our method compared to PAINT (Figure S9).

Since the exterior of the cell is almost entirely covered in a semi-crystalline S-layer of RsaA, we hypothesized that the majority of **9** was covalently attached to this protein (Figure S10). RsaA monomers are held tightly in the S-layer lattice, and we do not see evidence of SM diffusion in our raw data. The spatial organization of new RsaA incorporation is not fully understood. To view this, we performed pulse-chase labeling with **9**. Imaging the cells immediately after labeling shows random and even incorporation over the cell surface. If the cells are allowed to grow after the labeling and washing step, patches with no localizations appear in the reconstructions (Figures S11 and S12), indicating non-uniform insertion of new cell surface.

We report a rhodamine spirolactam capable of photoactivation at visible wavelengths and 3D super-resolution imaging. A

dx.doi.org/10.1021/ja508028h | *J. Am. Chem. Soc.* 2014, 136, 14003−14006

reactive ester version can be used to provide the context of the living cell surface to enhance other imaging experiments and as a method to study the growth of the bacterial S-layer. Other small-molecule fluorophores with controllable emission might be considered for cell surface studies. However, many of these dyes require additives like thiols or oxygen scavenging systems to photoswitch. These are not required for **9**, which has the additional advantage of apparent non-toxicity to the cells at the concentrations studied.

■ ASSOCIATED CONTENT

Supporting Information

Procedures, chemical synthesis, analysis, Figures S1−S12, and Movies S1 and S2. This material is available free of charge via the Internet at http://pubs.acs.org.

■ AUTHOR INFORMATION

Corresponding Author

wmoerner@stanford.edu

Notes

The authors declare no competing financial interest.

■ ACKNOWLEDGMENTS

The authors acknowledge Jared Schrader and the Lucy Shapiro laboratory for discussion and assistance in running protein gels. This work was supported in part by Grant No. R01-GM086196 from the National Institute of General Medical Sciences.

■ REFERENCES

(1) Cava, F.; Kuru, E.; Brun, Y. V.; de Pedro, M. A. *Curr. Opin. Microbiol.* **2013**, *16*, 731−737.

(2) Kuru, E.; Hughes, H. V.; Brown, P. J.; Hall, E.; Tekkam, S.; Cava, F.; de Pedro, M. A.; Brun, Y. V.; VanNieuwenhze, M. S. *Angew. Chem., Int. Ed.* **2012**, *51*, 12519−12523.

(3) Betzig, E.; Patterson, G. H.; Sougrat, R.; Lindwasser, O. W.; Olenych, S.; Bonifacino, J. S.; Davidson, M. W.; Lippincott-Schwartz, J.; Hess, H. F. *Science* **2006**, *313*, 1642−1645.

(4) Rust, M. J.; Bates, M.; Zhuang, X. *Nat. Methods* **2006**, *3*, 793−796.

(5) Hess, S. T.; Girirajan, T. P. K.; Mason, M. D. *Biophys. J.* **2006**, *91*, 4258−4272.

(6) Sharonov, A.; Hochstrasser, R. M. *Proc. Natl. Acad. Sci. U.S.A.* **2006**, *103*, 18911−18916.

(7) Dickson, R. M.; Cubitt, A. B.; Tsien, R. Y.; Moerner, W. E. *Nature* **1997**, *388*, 355−358.

(8) Fölling, J.; Belov, V.; Kunetsky, R.; Medda, R.; Schönle, A.; Egner, A.; Bossi, M.; Hell, S. W. *Angew. Chem., Int. Ed.* **2007**, *46*, 6266−6270.

(9) Heilemann, M.; Dedecker, P.; Hofkens, J.; Sauer, M. *Laser Photon. Rev.* **2009**, *3*, 180−202.

(10) Marriott, G.; Mao, S.; Sakata, T.; Ran, J.; Jackson, D. K.; Petchprayoon, C.; Gomez, T. J.; Warp, E.; Tulyathan, O.; Aaron, H. L.; Isacoff, E. Y.; Yan, Y. *Proc. Natl. Acad. Sci. U.S.A.* **2008**, *105*, 17789−17794.

(11) Uno, K.; Niikura, H.; Morimoto, M.; Ishibashi, Y.; Miyasaka, H.; Irie, M. *J. Am. Chem. Soc.* **2011**, *133*, 13558−13564.

(12) Subach, F. V.; Patterson, G. H.; Manley, S.; Gillette, J. M.; Lippincott-Schwartz, J.; Verkhusha, V. V. *Nat. Methods* **2009**, *6*, 153−159.

(13) Lord, S. J.; Conley, N. R.; Lee, H.-D.; Samuel, R.; Liu, N.; Twieg, R. J.; Moerner, W. E. *J. Am. Chem. Soc.* **2008**, *130*, 9204−9205.

(14) Schwering, M.; Kiel, A.; Kurz, A.; Lymperopoulos, K.; Sprödefeld, A.; Kramer, R.; Herten, D. *Angew. Chem., Int. Ed.* **2011**, *50*, 2940−2945.

(15) Vogelsang, J.; Cordes, T.; Forthmann, C.; Steinhauer, C.; Tinnefeld, P. *Proc. Natl. Acad. Sci. U.S.A.* **2009**, *106*, 8107−8112.

(16) Lee, M. K.; Williams, J.; Twieg, R. J.; Rao, J.; Moerner, W. E. *Chem. Sci.* **2013**, *4*, 220−225.

(17) Conley, N. R.; Biteen, J. S.; Moerner, W. E. *J. Phys. Chem. B* **2008**, *112*, 11878−11880.

(18) Dempsey, G. T.; Bates, M.; Kowtoniuk, W. E.; Liu, D. R.; Tsien, R. Y.; Zhuang, X. *J. Am. Chem. Soc.* **2009**, *131*, 18192−18193.

(19) Dempsey, G. T.; Vaughan, J. C.; Chen, K. H.; Bates, M.; Zhuang, X. *Nat. Methods* **2011**, *8*, 1027−1036.

(20) Heilemann, M.; van de Linde, S.; Schüttpelz, M.; Kasper, R.; Seefeldt, B.; Mukherjee, A.; Tinnefeld, P.; Sauer, M. *Angew. Chem., Int. Ed.* **2008**, *47*, 6172−6176.

(21) Patterson, G. H.; Lippincott-Schwartz, J. *Science* **2002**, *297*, 1873−1877.

(22) Ando, R.; Mizuno, H.; Miyawaki, A. *Science* **2004**, *306*, 1370−1373.

(23) Szent-Gyorgyi, C.; Schmidt, B. F.; Creeger, Y.; Fisher, G. W.; Zakel, K. L.; Adler, S.; Fitzpatrick, J. A. J.; Woolford, C. A.; Yan, Q.; Vasilev, K. V.; Berget, P. B.; Bruchez, M. P.; Jarvik, J. W.; Waggoner, A. *Nat. Biotechnol.* **2008**, *26*, 235−240.

(24) Thompson, R. E.; Larson, D. R.; Webb, W. W. *Biophys. J.* **2002**, *82*, 2775−2783.

(25) Lord, S. J.; Lee, H. D.; Moerner, W. E. *Anal. Chem.* **2010**, *82*, 2192−2203.

(26) Swulius, M. T.; Jensen, G. J. *J. Bacteriol.* **2012**, *194*, 6382−6386.

(27) Gahlmann, A.; Moerner, W. E. *Nat. Rev. Microbiol.* **2014**, *12*, 9−22.

(28) Knauer, K. H.; Gleiter, R. *Angew. Chem., Int. Ed.* **1977**, *16*, 113−113.

(29) Willwohl, H.; Wolfrum, J.; Gleiter, R. *Laser Chem.* **1989**, *10*, 63−72.

(30) Kim, H. N.; Lee, M. H.; Kim, H. J.; Kim, J. S.; Yoon, Y. *Chem. Soc. Rev.* **2008**, *37*, 1465−1472.

(31) Wu, L.; Dai, Y.; Marriott, G. *Org. Lett.* **2011**, *13*, 2018−2021.

(32) Chen, X.; Pradhan, T.; Wang, F.; Kim, J. S.; Yoon, J. *Chem. Rev.* **2012**, *112*, 1910−1956.

(33) Ram, S.; Prabhat, P.; Ward, E. S.; Ober, R. J. *Opt. Exp.* **2009**, *17*, 6881−6898.

(34) Juette, M. F.; Gould, T. J.; Lessard, M. D.; Mlodzianoski, M. J.; Nagpure, B. S.; Bennett, B. T.; Hess, S. T.; Bewersdorf, J. *Nat. Methods* **2008**, *5*, 527−529.

(35) Huang, B.; Wang, W.; Bates, M.; Zhuang, X. *Science* **2008**, *319*, 810−813.

(36) Greengard, A.; Schechner, Y. Y.; Piestun, R. *Opt. Lett.* **2006**, *31*, 181−183.

(37) Pavani, S. R. P.; Thompson, M. A.; Biteen, J. S.; Lord, S. J.; Liu, N.; Twieg, R. J.; Piestun, R.; Moerner, W. E. *Proc. Natl. Acad. Sci. U.S.A.* **2009**, *106*, 2995−2999.

(38) Thompson, M. A.; Lew, M. D.; Badieirostami, M.; Moerner, W. E. *Nano Lett.* **2010**, *10*, 211−218.

(39) Lew, M. D.; Lee, S. F.; Ptacin, J. L.; Lee, M. K.; Twieg, R. J.; Shapiro, L.; Moerner, W. E. *Proc. Natl. Acad. Sci. U.S.A.* **2011**, *108*, E1102−E1110.

(40) Badieirostami, M.; Lew, M. D.; Thompson, M. A.; Moerner, W. E. *Appl. Phys. Lett.* **2010**, *97*, 161103.

(41) Grover, G.; Pavani, S. R. P.; Piestun, R. *Opt. Lett.* **2010**, *35*, 3306−3308.

(42) Gahlmann, A.; Ptacin, J. L.; Grover, G.; Quirin, S.; von Diezmann, A. R. S.; Lee, M. K.; Backlund, M. P.; Shapiro, L.; Piestun, R.; Moerner, W. E. *Nano Lett.* **2013**, *13*, 987−993.

(43) Laub, M. T.; Shapiro, L.; McAdams, H. H. *Annu. Rev. Genet.* **2007**, *41*, 429−441.

(44) Amat, F.; Comolli, L. R.; Nomellini, J. F.; Moussavi, F.; Downing, K. H.; Smit, J.; Horowitz, M. *J. Bacteriol.* **2010**, *192*, 5855−5865.

(45) Jones, H. C.; Schmidt, J. M. *J. Bacteriol.* **1973**, *116*, 466−470.